Sensors and Materials, Vol. 19, No. 1 (2007) 057–078
MYU Tokyo

S & M 0666

Electrostatically Driven 3-Way Silicon Microvalve for Pneumatic Applications

Stephan Messner[1,*], Jochen Schaible[2], Peter Nommensen[1] and Roland Zengerle[1,3]

[1]HSG-IMIT, Wilhelm-Schickard-Str. 10, D-78052 Villingen-Schwenningen, Germany
[2]Hoerbiger Automatisierungstechnik GmbH, Südliche Römerstrasse 15, D-86972 Altenstadt, Germany
[3]IMTEK, University of Freiburg, Georges-Köhler-Allee 103, D-79110 Freiburg, Germany

(Received January 6, 2006; accepted: February 5, 2007)

Key words: microvalve, electrostatic actuation, micromachining, pneumatics

In many industrial applications there is a need for microvalves meeting requirements like small form factor, low weight, high flow rate, short response time and low power consumption. Especially for pneumatic applications, there is a need for microvalves with a normally-closed, 3-way functionality. In this paper, we present a microvalve which meets the requirement described above and which is used in a gas chromatography application due its small dead volume. At the moment, it is used in a space flight mission because of its resistance against mechanical vibration and variation in temperature. The microvalve is fabricated by silicon micromachining including a three layer full wafer bond process. The silicon chip stack is mounted onto a ceramic substrate which is covered by a plastic cap. To control the valve a low power driver electronics chip, able to convert TTL levels to the actuation voltage of 200 V is assembled directly on top of the microvalve. Due to the electrostatic actuation principle and the low power electronics, the peak power consumption of the valve is below 10 mW and the response time is less than 1 ms. The flow rate of the microvalve is in the range of 500 sccm and the presented version is designed to operate in a pressure range of up to 8 bar.

1. Introduction

In many industrial fields, especially in automation, there is a trend towards decentralisation and intelligent, stand-alone operating sub systems. A pneumatic cylinder containing microvalves, sensors and control electronics could be such a sub system which

*Corresponding author, e-mail address: stephan.messner@hsg-imit.de

is able to carry out commands independently as well as doing self diagnostics. Ideally such a cylinder only needs the pneumatic interfaces for the pressurized air and an electronic interface for information exchange, but no additional interface for electrical power. This trend leads to the need of miniaturized components with low power consumption meeting the requirements for industrial applications. Microvalves for industrial, pneumatic applications must have a 3-way normally-closed functionality, a high air flow, a low leakage rate, a short response time, a wide temperature range (–40 to 80°C) and have to operate in the standard pressure range of 0 to 8 bar (8×10^5 Pa). To work in sub systems with power provided for example by serial interfaces the power consumption has to be as low as possible. To enable the integration in sub systems like pneumatic cylinders, the outer dimensions of the valve have to be as small as possible. Ideally the form factor should be compatible with standard pneumatics, where the width of the valves is standardized and 10 mm is the smallest standard at present.

In the past several microvalves with different actuation principles were presented.[1–8] All of these valves show very good properties for special applications, but up to now there is no microvalve which meets all the requirements mentioned before. A very important requirement for pneumatic applications is the 3-way normally-closed functionality of the valve. Beside inlet and outlet port, 3-way valves embody a third port, the exhaust. The inlet port is connected to the pressure supply, the outlet port is connected to the load (e.g., a pneumatic cylinder). The exhaust is connected to ambient. In the normal, unactuated state the inlet port of normally-closed 3-way valves is blocked and the outlet is connected to the exhaust. In the actuated state the pressure (inlet port) is connected to the outlet port while the port to ambient is blocked. By switching between these two states the pressure at the outlet can be switched between supply pressure and ambient pressure which enables pneumatic work to be performed at the outlet port (e.g., move a pneumatic cylinder).

The electrostatically driven microvalve we are presenting is the first normally-closed 3-way electrostatically driven microvalve. Figure 1 shows a photograph of the microvalve with removed plastic cap.

2. Design and Layout

The design of the 3-way microvalve is an advancement of the 2-way design we presented earlier.[9] Figure 2 shows a cross-section of the 3-way silicon microvalve chip fabricated by silicon micromachining.

The silicon microvalve itself consists of three layers. The bottom chip contains the outlet and the exhaust port. The movable valve plate is part of the plate chip and the cover chip contains the pressure (inlet) port. In order to realize a normally-closed valve function the pressure port must be sealed against an inlet pressure of up to 8 bar (8×10^5 Pa) in the unactuated state of the valve. This task is done by pre-stressing the valve plate. The valve seat of the pressure port is raised by a few micrometers (z_p) with reference to the outer area of the chip. This elevation is realised by wet chemical etching of the outer area of the chip. When mounting the cover chip to the plate chip the raised area leads to a deflection of the valve plate and thus to a pre-stressed valve plate suspension which works as a spring.

The normally closed function is guaranteed when the restoring force of the pre-stressed suspension is higher than the force resulting from the inlet pressure. The electrostatic

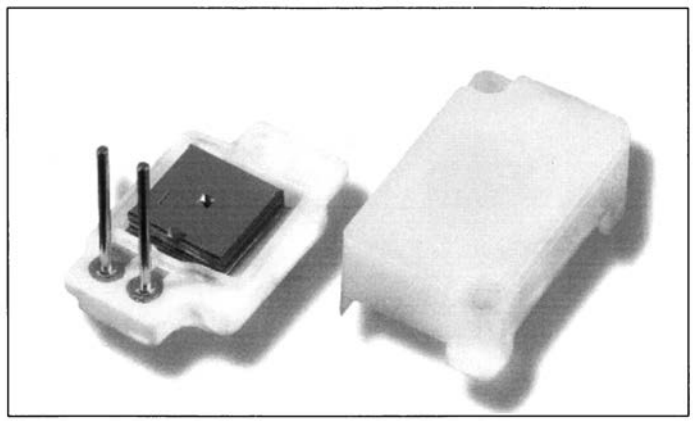

Fig. 1. Photograph of the microvalve with removed plastic cap.

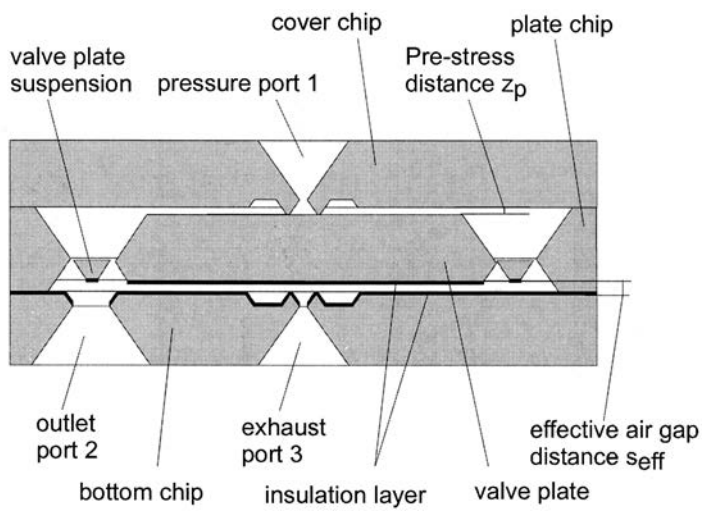

Fig. 2. Cross-sectional, schematic view of the silicon microvalve.

actuation principle was chosen for its low power consumption, independence from the ambient temperature, fast response time and unique possibility for integration within silicon bulk micromachining. By applying a voltage between bottom and plate chip, an electrostatic field is generated in the air gap between valve plate and bottom chip. The resulting electrostatic force moves the valve plate towards the bottom chip. An insulation layer prevents short circuits. The deflection of the valve plate leads to a resulting force of the valve plate suspension which works against the electrostatic force. Figure 3 shows a schematic drawing of the plate chip.

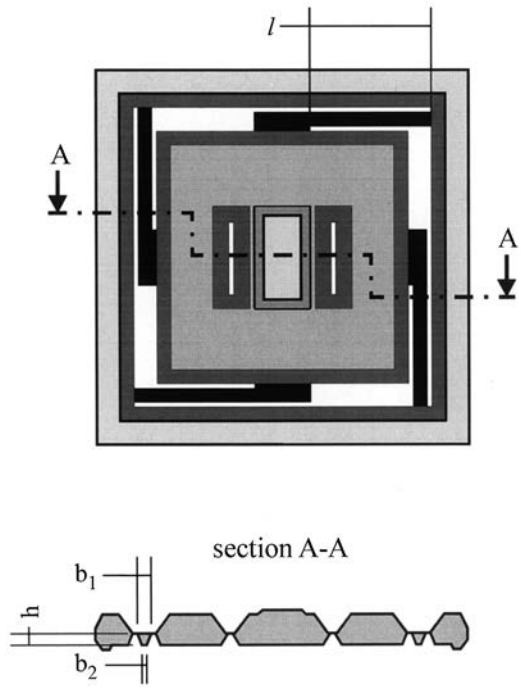

Fig. 3. Schematic drawing of the plate chip.

The valve plate is suspended on four elastic beams having a trapezoid shape. The reset force of the valve plate suspension can be calculated as follows:

$$F_{\text{res}} = k \cdot z \tag{1}$$

where z is the actual deflection of the valve plate and k is the stiffness (spring constant) of the suspensions. For the small deflection of the beam, which is below 5% of its thickness, a linear spring constant can be assumed. For the trapezium shape it can be calculated according to the following equation:

$$k = \frac{4}{3} \cdot \frac{E}{1-\nu^2} \cdot \frac{(b_1^2 + 4b_1b_2 + b_2^2) \cdot h^3}{(b_1 + b_2) \cdot l^3} \tag{2}$$

where E is the Young's modulus and ν is Poisson's ratio. The geometrical parameters b_1, b_2, h and l are the geometrical dimensions of the trapezium shaped elastic beams and are shown in Fig. 3.

The electrostatic force, induced by the applied electrical field can be calculated using the following equation:

$$F_{\mathrm{elst}} = \frac{1}{2} \cdot \frac{\varepsilon_0}{\kappa_{\mathrm{air}}} \cdot A_{\mathrm{el}} \cdot U_e^2 \cdot \frac{1}{\left(\frac{d_{\mathrm{in}}}{\kappa_{\mathrm{in}}} + \frac{s - z}{\kappa_{\mathrm{air}}} \right)^2} \tag{3}$$

where ε_0 is the permittivity, κ_{air} and κ_{in} are the dielectric constants for air and the insulation layer. A_{el} is the electrostatically active surface, U_{e} is the voltage applied, d_{in} is the thickness of the insulation layers and s is the initial air gap height. The equilibrium of the mechanical reset force (eq. (1)) and the electrostatic actuation force (eq. (3)) considering eq. (2) leads to the following equation where $s_{\mathrm{eff}} = s + d_{\mathrm{in}}/\kappa_{\mathrm{in}}$ is the effective air gap distance between the electrodes (valve plate / bottom chip) and it is assumed that $\kappa_{\mathrm{air}} = 1$.

$$z^3 - 2 \cdot s_{\mathrm{eff}} \cdot z^2 + s_{\mathrm{eff}}^2 \cdot z - \frac{1}{2} \cdot \frac{\varepsilon_0 \cdot A_{\mathrm{el}}}{k} \cdot U_{\mathrm{e}}^2 = 0 \tag{4}$$

This equation describes the deflection of the valve plate depending on the electrical voltage applied. In the range $0 \le z/s_{\mathrm{eff}} < 1/3$ the deflection z of the valve plate is stable, for $z/s_{\mathrm{eff}} \ge 1/3$ the deflection is unstable[12] and the valve plate snaps down to the bottom chip and seals the exhaust. The solution of the cubic eq. (4) leads to the switching voltage where the deflection gets unstable of:

$$U_{\mathrm{S}} = \sqrt{\frac{8}{27} \cdot \frac{k \cdot s_{\mathrm{eff}}^3}{\varepsilon_0 \cdot A_{\mathrm{el}}}} \tag{5}$$

In the case of the design presented in Fig. 2 the pre-stress distance z_p has to be considered which is leading to eq. (6).

$$U_{\mathrm{S}} = \sqrt{\frac{8}{27} \cdot \frac{k \cdot (s_{\mathrm{eff}} + z_{\mathrm{p}})^3}{\varepsilon_0 \cdot A_{\mathrm{el}}}} \tag{6}$$

If the voltage applied to the microvalve is higher than U_{s}, the valve plate snaps down to the bottom chip and seals the exhaust. To keep the switching voltage in a reasonable range of below 200 V the air gap distance has to be less than 5 μm, considering that k is 50 kN/m, A_{el} is 15 mm^2 and z_p is 2.5 μm.

The force induced by the pneumatic pressure is not considered in eq. (1) because it acts in the same direction as the electrostatic force and leads to a reduced switching voltage. Thus, in terms of the switching voltage eq. (1) represents the worst case when no pressure is applied to the valve. Consequently, the valve plate suspensions have to be weak enough,

so that the relatively low electrostatic force is sufficient to deflect the valve plate. On the other hand, when the maximum pressure of 8 bar (8×10^5 Pa) is applied and the electrostatic field is off, the valve plate suspensions have to be stiff enough to move the valve plate back.

To minimize the forces induced by the pneumatic pressure on the valve plate, the valve is designed in a way that the pressure difference between inlet and outlet only works on the small area within the valve seat area. Thus, a high pneumatic pressure can be controlled using a relatively small electrostatic force as earlier presented by Huff *et al.*[5]

The flow rate of the valve is mainly influenced by the highest flow resistance in the valve which is in the area of the valve seats and is determined by the smallest cross-section for the air flow. Taking the very small air gap distance into account the smallest cross-section for the flow is determined by the perimeter length of the valve seat multiplied with the air gap distance. To achieve a maximum flow rate, the perimeter length of the valve seat has to be as long as possible but keeping the enclosed area of the valve seat as small as possible. This approach to increase the flow rate of microvalves was already earlier presented in refs. 18–21. One method to increase the perimeter length while keeping the enclosed surface constant is to use a meandered valve seat as presented in refs. 9–11. Another method to optimise the flow rate of microvalves is to use multiple orifices and thus to increase the ration between perimeter length to enclosed area of the valve seat. This approach was presented in refs. 13, 16 and 17 and could be used for further optimisation of the microvalve presented here.

To be able to estimate the flow rate of the microvalve by analytical means, some assumptions and simplifications are necessary. It is assumed that the velocity of the inflowing gas is negligible compared to the velocity at the smallest cross-section (nozzle). Thus, a steady state expansion flow can be presumed.

Furthermore, it is assumed that the change of state is isentropic. After ref. 14, these assumptions lead to the following eq. (7):

$$\dot{m}_{th} = \mu_{\mathrm{M}} \cdot A_{\mathrm{M}} \cdot \psi_{\mathrm{A},2} \cdot \sqrt{2 \cdot \frac{p_{1'}}{v_1}} \tag{7}$$

This equation describes the mass flow through a nozzle, where μ_{M} is an empirically determined factor taking into account friction and the shape of the nozzle. A_{M} is the area of the smallest cross-section (nozzle). The absolute pressure at the inlet of the valve is p'_1 and $v_1=1/\rho_1$ is the reciprocal value of the gas density at the inlet of the valve. $\psi_{A,2}$ is a nondimensional term and calculated from the following equation:

$$\psi_{\mathrm{A},2} = \sqrt{\frac{\gamma}{\gamma-1}\left[\left(\frac{p_{2'}}{p_{1'}}\right)^{\frac{2}{\gamma}} - \left(\frac{p_{2'}}{p_{1'}}\right)^{\frac{\gamma+1}{\gamma}}\right]} \tag{8}$$

$\psi_{A,2}$ is only depending on the ratio between the absolute pressure at the outlet p'_2 and the

absolute pressure at the inlet p'_1 and the adiabatic exponent γ which is the ratio of specific heats c_p / c_v and depending on the type of gas (γ=1.4 for air). $\psi_{A,2}$ has a parabolic shape starting at $\psi_{A,2} = 0$ for a pressure ratio $p'_2 / p'_1 = 1$. If the pressure ratio is decreasing, $\psi_{A,2}$ increases up to its maximum

$$\psi_{A,max} = \left(\frac{2}{\gamma + 1} \right)^{\frac{1}{\gamma - 1}} \cdot \sqrt{\frac{\gamma}{\gamma + 1}} \tag{9}$$

at the Laval (or critical) pressure ratio of:

$$P_{kr} \equiv P_L = \left(\frac{2}{\gamma + 1} \right)^{\frac{\gamma}{\gamma - 1}} \tag{10}$$

If the pressure ratio decreases further, $\psi_{A,2}$ and thus the mass flow through the nozzle stays constant.

For pneumatic valves the volume flow $\dot{V}$ is used to specify the flow characteristic of valves. Since it depends on the actual pressure, the temperature and the density of the medium the volume flow with reference to standard conditions (p'_s, T_s see Table 1) is used. The standard volume flow (standard flow rate) $\dot{V}_S$ can be calculated using the following equation:

$$\dot{V}_S = \frac{\dot{m}}{\rho_S} = \frac{R \cdot T_S}{p'_S} \cdot \dot{m} \tag{11}$$

The mass flow through a nozzle is the same at each position (before and behind). The standard flow rate depends on the density ρ_s, respectively the gas constant R, the temperature T_s and the absolute pressure p'_s. Using eq. (11) the standard volume flow through the microvalve can be calculated to be $\dot{V}_S$ = 556 sccm (standard cubic centimetres per minute) considering the parameters, listed in Table 1. The area of the smallest cross-section

Table 1
List of parameters for the calculation of the volume flow.

Parameter	p'_1	p'_2,p'_S	A_M	µm	γ	R	T_S
	(Pa)	(Pa)	(m^2)	(l)	(l)	$\left(\frac{J}{kg \cdot K} \right)$	(K)
Value	7×10^5	1.013×10^5	1.125×10^{-8}	0.6	1.4	287	293.15

(nozzle) A_M in Table 1 is calculated by the perimeter length of the valve seat $P_v = 3.75\times10^{-3}$ m multiplied with the air gap distance $s = 3\times10^{-6}$ m. The calculated volume flow rate is valid for the flow from the pressure port to the outlet port in the actuated state of the valve as well as for the flow from the outlet port to the exhaust in the not actuated state of the valve. In this calculation only the biggest flow resistance in the area of the valve seat is taken into account. Further flow resistances are considered neglected. Also, the reduction of the air gap distance as a consequence of the inlet pressure causing a warpage of the cover chip is not considered in the calculation. Taking these simplifications into account, the measured flow rate should be smaller than the calculated value.

3. Fabrication

The actual microvalve is manufactured by silicon bulk micromachining. The three silicon layers are structured separately by wet and dry etching technologies. In the following, the process steps for the three layers are described.

3.1 *Bottom chip wafer*

For the fabrication of the bottom chips, a double side polished (100)-oriented *n*-doped silicon wafer with a thickness of 525 µm and a resistivity of 1–10 Ωcm is used. In a first step the wafer is coated with a silicon dioxide layer (Fig. 4(a)) acting as a mask for the following wet-etching. After coating both wafer sides with a photo resist, the structures of the first mask are exposed to the top side (TS) of the wafer (Fig. 4(b)). In the following step, the silicon dioxide layer is removed in the exposed areas and after that, the photo resist is removed from both sides of the wafer (Fig. 4(c)).

A 33% potassium hydroxide solution (KOH) at 60°C is used to etch the structures of the first mask into the TS of the silicon wafer (Fig. 4(d)). The resulting structures act as spacers (not visible in Fig. 2) to prevent sticking of the valve plate to the bottom chip in the microvalve. In the next step, both sides of the wafer are coated with a double layer of silicon dioxide and silicon nitride, acting as the mask for the following KOH-etching. The second mask is exposed to the bottom side (BS) of the wafer and the silicon nitride is structured by a dry etching process. The silicon dioxide layer which lies beneath, is removed by a wet chemical process (Fig. 4(e)). In the following KOH-etch process (at 80°C) deep cavities are structured into the BS of the wafer. After that, the silicon dioxide / nitride double layer is removed from both sides by wet chemical etching (Fig. 4(f)).

After the deposition of a silicon dioxide layer on both sides of the wafer an the exposure of the third mask, the valve seats are structured from the TS of the wafer using a deep reactive ion etching (DRIE) process (Fig. 4(g)). The silicon dioxide layer on the BS acts as the stop layer for the DRIE process and prevents a break through in the areas of the outlet and exhaust ports (see Fig. 2). In the last step, the remaining silicon dioxide is removed by wet chemical etching.

3.2 *Valve plate wafer*

For the fabrication of the valve plate chips, a double side polished (100)-oriented *n*-doped silicon wafer with a thickness of 525 µm and a resistivity of 1–10 Ωcm is used. In

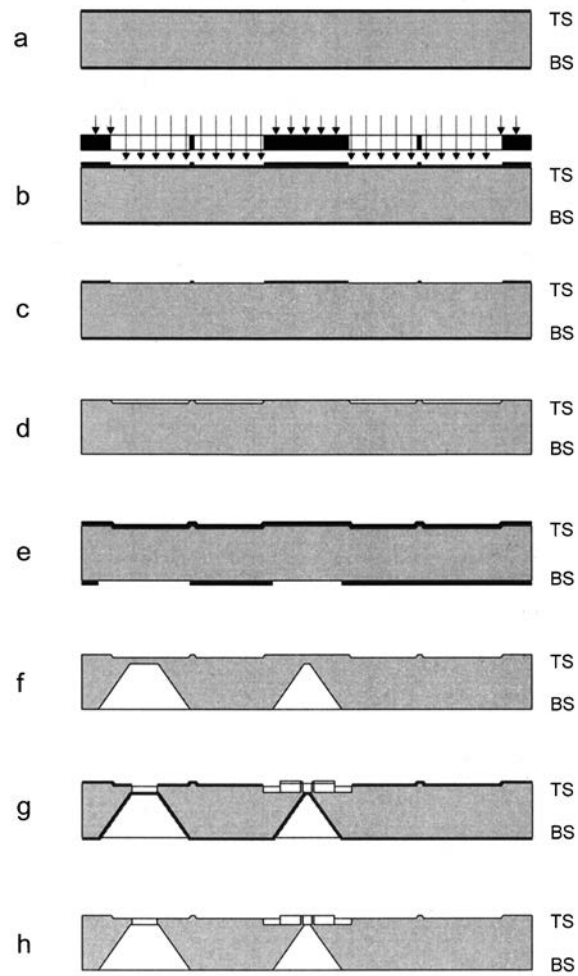

Fig. 4. Schematic drawing of the process sequence for the fabrication of the bottom chips.

the first step, the wafer is coated with a silicon dioxide layer. After exposing the first mask to the BS of the wafer (Fig. 5(a)), 5 μm deep cavities are KOH-etched (at 60°C) into this side (Fig. 5(b)). The depth of these cavities later defines the air gap distance of the microvalves (see Fig. 2).

After the deposition of a silicon oxide / nitride double layer on both sides, the second mask is exposed to the TS and the double layer is opened in the exposed areas (Fig. 5(c)). After that, a second silicon oxide / nitride double layer is deposited on both sides and the

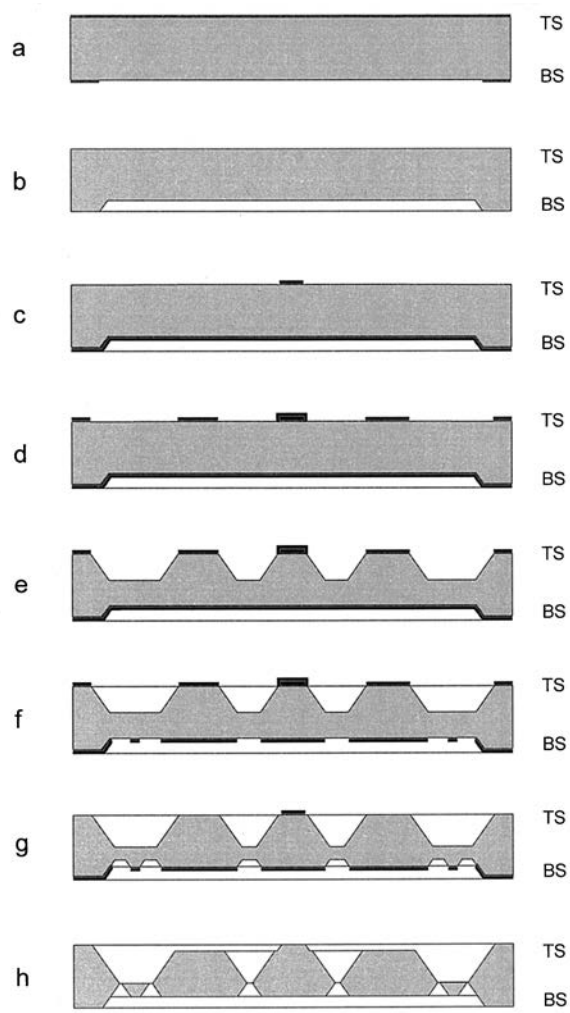

Fig. 5. Schematic drawing of the process sequence for the fabrication of the valve plate chips.

After that, a second silicon oxide / nitride double layer is deposited on both sides and the third mask is exposed to the TS of the wafer. The top silicon nitride layer is removed in the exposed areas from the TS and on the complete wafer area on the BS using a dry etching process. The silicon oxide beneath is afterwards removed by wet-etching (Fig. 5(d)). After that, the silicon wafer is KOH-etched (at 80°C) from the TS (Fig. 5(e)) and the fourth mask is deposited and structured from the BS. In the next step the KOH-etching is continued from both sides until the skinniest area has a thickness of about 50 μm. After that, the top

silicon dioxide / nitride double layer from the TS of the wafer is removed.

With this step, the silicon dioxide / nitride double layer beneath, containing the structures of the second mask (see above) is uncovered (Fig. 5(g)). The KOH-etching is now continued until the valve plate and the valve plate suspensions are completely formed. In the last step, the silicon dioxide / nitride double layer is completely removed from both sides by wet-etching (Fig. 5(h)).

3.3 *Cover chip wafer*

For the fabrication of the valve plate chips, a double side polished (100)-oriented *n*-doped silicon on insulator (SOI) wafer with a total thickness of 525 µm and a resistivity of 1–10 Ωcm is used. The thickness of the buried oxide is 200 nm and the thickness of the silicon layer on top of the oxide is 2 µm (Fig. 6(a)).

In the first step a silicon dioxide / nitride double layer is deposited on both sides of the

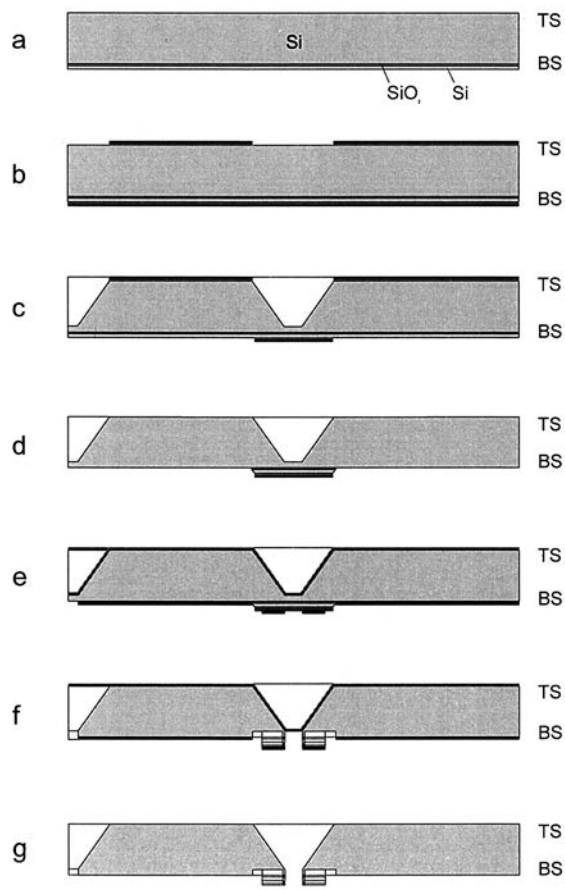

Fig. 6. Schematic drawing of the process sequence for the fabrication of the cover chips.

exposed areas (Fig. 6(b)). In the following step, cavities are etched from the TS of the wafer, using the wet-chemical KOH-process at 80°C. In the next step, the second mask is exposed to the BS. After removing the silicon dioxide / nitride double layer in the exposed areas of the BS (Fig. 6(c)), the KOH-etching is continued on both sides until the buried silicon dioxide layer is uncovered. In the following step, the silicon nitride layer on the TS of the wafer is removed by a dry etching process. After that, the uncovered oxide layer on the BS and the oxide layer on the TS are removed by a wet-chemical process step (Fig. 6(d)). In the next step, only the TS of the wafer is coated with silicon dioxide using a PECVD-process. After coating the BS with a photo resist, the third mask is exposed to this side of the wafer. This mask is used to structure the valve seats of the cover chips. Therefore, at first, a dry etching process is used to remove the silicon dioxide / nitride double layer which is still existing in the middle of the cover chips. After that, the 2 μm thick silicon layer is removed by DRIE. This process stops at the buried oxide layer which is in the following process step removed by dry etching. The DRIE process is then continued and the structures of the third mask (containing the valve seat structures) are etched into the silicon wafer from the BS (Fig. 6(f)). The silicon dioxide on the TS acts as the stop layer for the DRIE process and prevents a breakthrough in the area of the pressure port (see Fig. 2). The photo resist on the BS of the wafer is removed by a plasma process. To remove the silicon dioxide on the BS a wet-etch process is used (Fig. 6(g)).

The resulting valve seat structures in the middle of the chips are raised by 2.5 μm ± 0.2 μm (*zp*) with reference to the outer area of the chip.

When bonding the three wafers (bottom, valve plate and cover chip wafer) together, this raised area deflects the valve plates and thus creates the pre-stressing of the valve plate suspensions. The silicon nitride layer, which is on top of the valve seat structure of the cover chips prevents a bonding of the valve seat structures to the valve plates and thus guarantees its movability.

3.4 *Full wafer bonding and packaging*

After structuring, the valve plate wafer is coated with an insulation layer (silicon dioxide) of 1 μm thickness, which is also used as the bonding layer for the silicon wafer bonding process. In the next step, the three wafers (bottom, valve plate and cover chip wafer) are cleaned in order to obtain hydrophilic wafer surfaces. A silicon wafer bond process is used to bond the three wafers together. In a first step of this process the wafers are aligned and stacked one upon the other. The mask-and bond-aligner of Electronic Visions type AL6-2RG is used for this process step. Then, the wafer stack is pressed together using the full wafer bonder type EV500 of Electronics Visions, in order to bring the wafers in contact and to pre-stress the valve plate suspensions. In the next step, the wafer stack is annealed at 1100°C for 3 h in nitrogen atmosphere.

A dry etch process is used, to remove the silicon dioxide from the area, where the valve plate chip has to be electrically contacted (by wire bonding) in the following packaging process (see Fig. 7). After that, aluminium is sputtered to both sides of the wafer stack to enable the electrical contacting of the valve in the packaging process afterwards. After mounting the wafer stack on a sawing tape, it is diced into separate chips using a dicing saw. To prevent water contamination from the saw, the wafer stack is covered by a

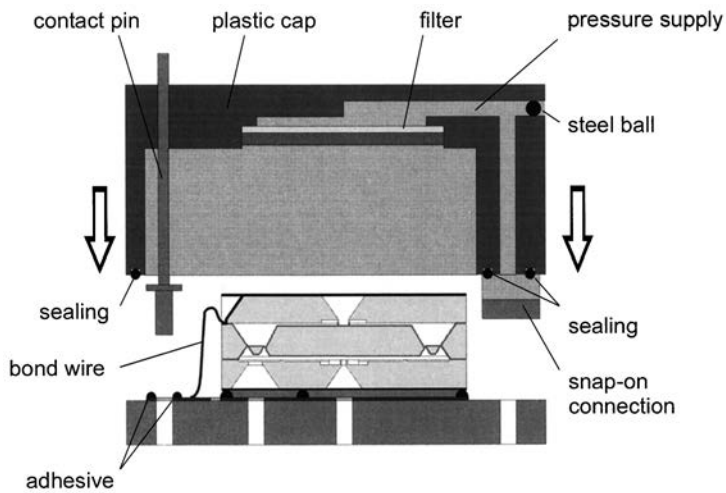

Fig. 7. Packaging concept of the microvalve.

transparent tape which is mounted on top. A thorough investigation of the microvalves showed, that water inside a microvalve after dicing is solely caused by failures from the full wafer bond process. This water can be optically detected in the form of small droplets at the inner side of the tape covering the cover chip wafer during the dicing process. Valves which show such droplets after dicing have to be sorted out. This is a simple method to monitor the quality of the bonding process.

Figure 8 shows the packaging concept. The silicon valve chip is mounted to a ceramic substrate which contains two metal pads made by screen printing. The bottom chip of the valve is connected to the first pad using electrically conductive adhesive. The plate chip is connected to the second pad by wire bonding. The two pads are connected to contact pins also using electrically conductive adhesive. The contact pins are used as the external electrical interface to the valve.

All three pneumatic ports are at the bottom side of the ceramic substrate. The outlet and exhaust port of the ceramic substrate are directly connected to the outlet and exhaust of the silicon valve chip. The seal between the outlet and exhaust is realized by the gluing process which is also used to mount the valve chip to the ceramic substrate and to electrically contact the bottom chip as described above. This seal is not shown in Fig. 8. The pressure port of the ceramic substrate is connected to a small channel inside the plastic cap which conducts the pressure through a particle filter to the top side of the valve (Fig. 7). The filter is made of a polysulphone membrane with a pore size of 0.2 μm. Due to the fact, that the plastic cap is made by injection moulding, the small channel inside the plastic cap has an opening to the side of the cap (see Fig. 7). A steel ball is pressed into this opening in order to close it.

The plastic cap is mounted to the ceramic substrate using snap-on connections. A seal between ceramic substrate and plastic cap prevents leakage. The completely assembled

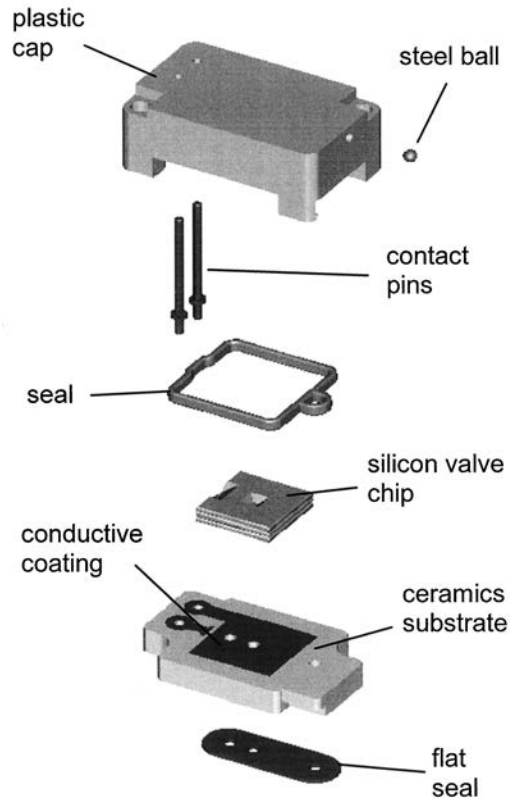

Fig. 8. Cross-sectional view of the microvalve assembly.

microvalve can be mounted onto an adapter block using screws. A flat seal between valve and adapter block prevents leakage and "cross-talk" between the different ports. The outer dimensions of the valve chip are 6×6×1.5 mm^3, the outer dimensions of the packaged valve are 16×10×7 mm^3.

A driver electronics which converts a 3 V input voltage into 200 V output voltage is placed on top of the completely assembled microvalve. The overall power consumption is approximtely 10 mW. Figure 9 shows the completely assembled microvalve with the unpackaged driver electronics on top.

4. Measurement Results

To characterize a 3-way valve different measurements have to be carried out. The pressure values p_1, p_2 and p_3 used in the following are pressure values relative to ambient pressure. Figure 10 shows the typical flow rate from the pressure port to the outlet port.

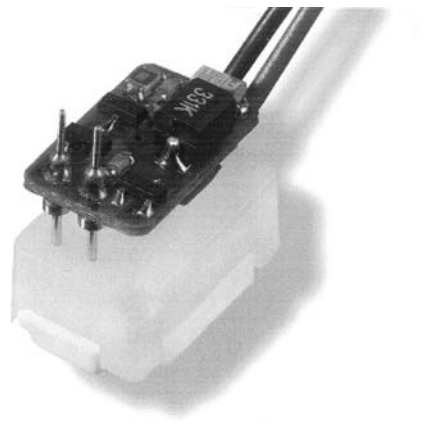

Fig. 9. Completely assembled 3-way microvalve with driver electronics mounted on top.

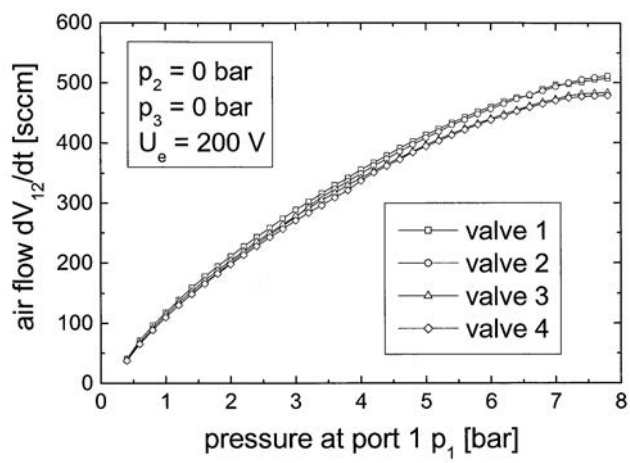

Fig. 10. Measured flow rate from pressure to outlet port versus pressure at pressure port (1 bar = 10^5 Pa).

Four different valves of the same type were measured. Due to the high quality full-wafer-bond only small variations occur between the different valves of the same type. The principal setup used for this measurement is shown in Fig. 11. The measurements were taken, with a voltage of U_e = 200 V applied to the valve. In this state the exhaust port is blocked by the valve plate and air flows from the pressure port to the outlet port. Outlet

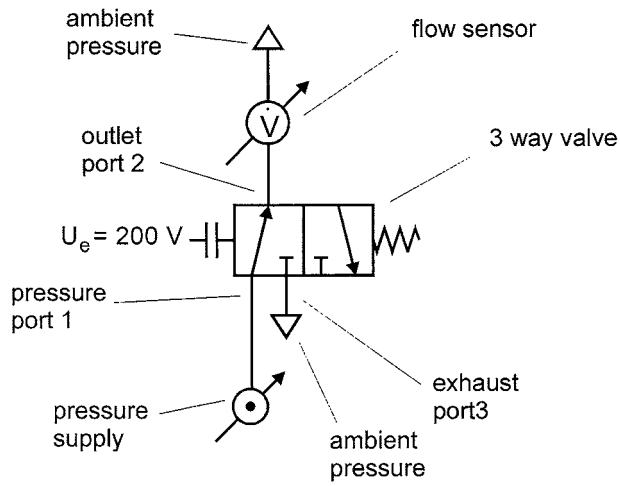

Fig. 11. Setup for the measurement of the flow rate from pressure port 1 to outlet port 2.

port and exhaust port are connected to ambient pressure. The flow rate is measured at the outlet port. At a pressure difference of 6 bar (6×10^5 Pa), which is the standard pressure for pneumatic applications, the air flow is approximately 475 sccm.

In Fig. 12 the leak rate at the exhaust port for the above mentioned state of the valve is shown. The setup for this measurement is shown in Fig. 13. At a pressure difference of 6 bar the leak rate is below 1 sccm which is approximately 0.2% of the maximum flow rate. The noise in the measurement results for higher pressures is caused by the measurement precision of the flow meter which was used, because the leak rate of the microvalve is at the bottom of its measurement range. For low pressures the leak rate increases. The reason for this is, that the applied pressure leads to a force on the valve plate and supports the sealing at the valve seat of the exhaust port. Thus, if the pressure gets higher, the force on the valve plate increases and the sealing is better.

In the basic state of the valve, with no voltage applied, the pressure port is blocked by the valve plate. The air flows from the outlet port to the exhaust port where the air flow is measured. To perform this measurement, the pressure is simultaneously applied to the outlet port and pressure port. Figure 13 in principle shows this measurement setup. The only difference is that the applied voltage is $U_e = 0$ V. The maximum flow rates for the four measured valves vary between 350 and 450 sccm (see Fig. 14). The flow rate decreases for pressures above 6 bar, contrary to what normally would be expected. The reason for this is the pressure difference between inside and outside the silicon microvalve which causes a warpage of the cover chip and thus a reduction of the air gap distance at the valve seat and consequently a decrease in flow rate. The pressure inside the silicon microvalve is lower than the applied pressure, because of internal flow resistances.

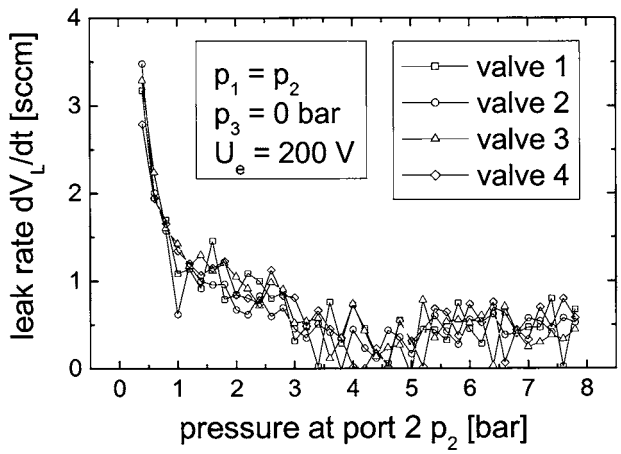

Fig. 12. Leak rate at exhaust versus pressure at outlet port 2.

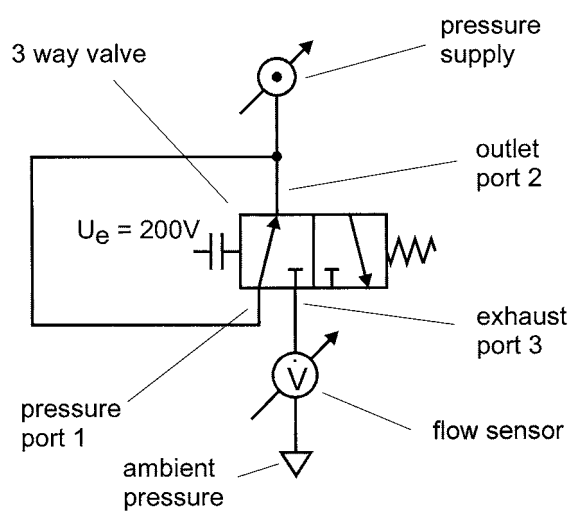

Fig. 13. Setup for the measurement of the leak rate to the exhaust port 3.

Figure 15 shows the typical hysteresis of the electrostatic actuation principle. The air flow from the pressure port to the outlet port versus the applied voltage is shown. The setup shown in Fig. 11 is used for this investigation. When no voltage is applied the valve plate

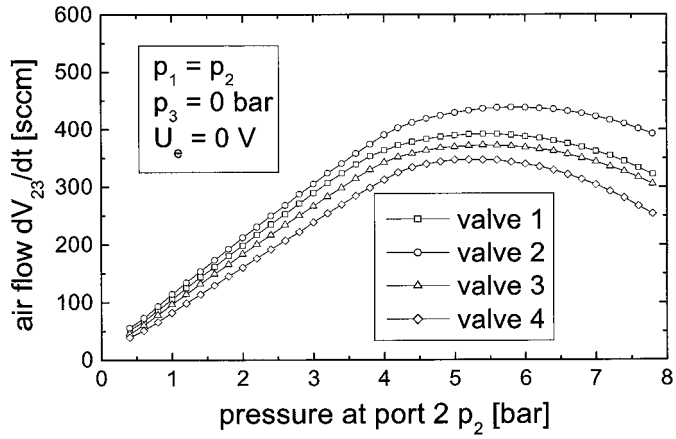

Fig. 14. Measured flow rate from outlet to exhaust port versus pressure at outlet port (1 bar = 10^5 Pa).

seals the pressure port. At the switching voltage $U_{s,1}$ of about 60 V the valve plate snaps in its second stable position and seals the exhaust port. The air flow from inlet port to outlet port is approximately 475 sccm. The voltage $U_{s,2}$ where the valve plate moves back in its original position is lower, because the effective distance s_{eff} between the electrodes is lower than in the original position. Thus the electrostatic force at a given voltage is higher.

The switching voltage $U_{s,1}$ depends on the inlet pressure, because the inlet pressure induces a force to the valve plate. Figure 16 shows the mean values of $U_{s,1}$ and $U_{s,2}$ vs the pressure at the pressure port of the four measured valves. The variations in the measurement results are caused by fabrication tolerances and the measurement accuracy. The pressure dependence of the switching voltage $U_{s,1}$ can clearly be seen. $U_{s,2}$ also depends on the inlet pressure. The pressure difference between inside and outside of the silicon microvalve causes a deformation which leads to a change in the effective distance of the electrodes and thus to a change in $U_{s,2}$. Electrostatic charging of the dielectric, which occurs during operation of the valve and leads to a change in the switching voltage, is a known problem for electrostatic micro actuation units.[15] To prevent this effect, the driver electronics was designed in a way, that the polarity of the output voltage is reversed every time, a voltage is applied to the valve. If the voltage is applied for a longer period, the polarity of the voltage is reversed every second.

In Fig. 17 the mechanical response time of the valve plate is shown. The movement of the valve plate was measured by using an optical distance sensor. For this measurement, the cover chip was removed from the valve to provide access to the valve plate. This investigation was carried out at atmospheric pressure. By applying a step function input of 200 V between bottom and plate chip the valve plate moves within less than 0.5 ms.

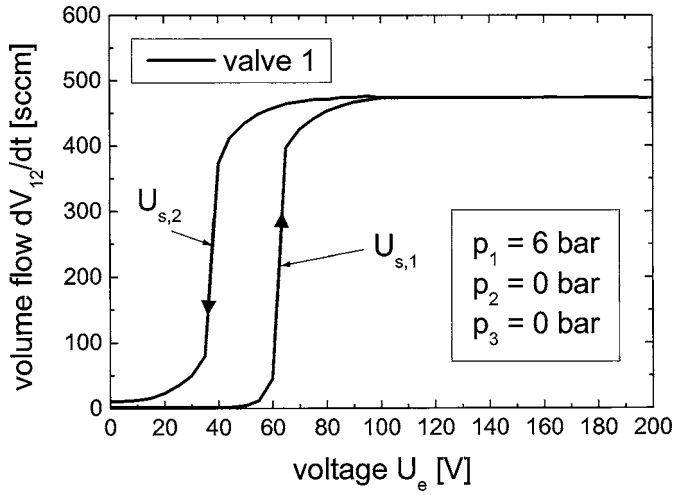

Fig. 15. Flow rate from pressure to outlet port vs applied voltage.

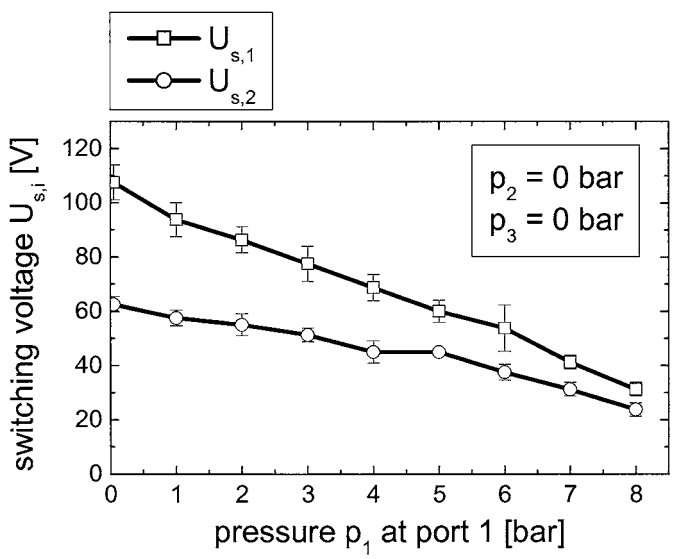

Fig. 16. Switching voltages $U_{s,1}$ and $U_{s,2}$ versus pressure at pressure port 1.

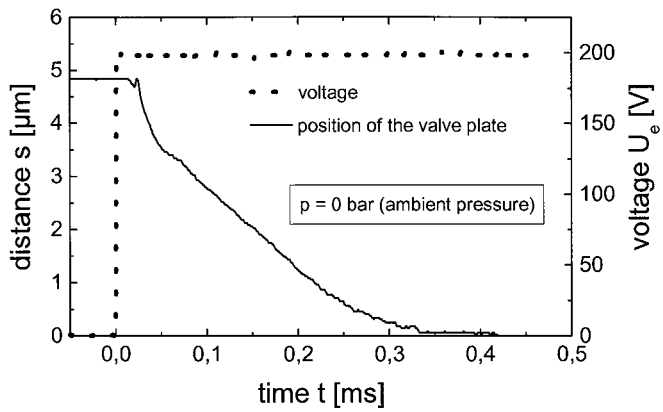

Fig. 17. Mechanical response time of the valve plate.

5. Conclusion

We have presented a normally-closed 3-way silicon microvalve meeting industrial requirements such as small size, fast switching times and low power consumption. It was shown that this valve is able to control the required pressure of 6 bar which is used as a standard in industry. The overall power consumption of the valve is less than 10 mW, enabling the simple control of the valve using logic signals (3–5 V, ~2 mA) without an additional power supply.

The valve chips were completely fabricated using silicon micromachining. The 3 layer wafer stack was bonded by a silicon wafer bond process, generating a pre-stress to the valve plate in order to seal the pressure port against a pneumatic pressure of up to 8 bar (8×10^5 Pa). It can be seen from Figs. 10, 13, 14 and 16 that the fabrication on full wafer level results in a very good homogeneity of the manufactured valves.

Acknowledgements

The authors would like to thank the state of Baden-Württemberg (Germany) and the Landesstiftung Baden-Württemberg gGmbH for the financial support of this research.

References

1 J. H. Jerman: Proc.Transducers 91 (IEEE, Piscataway, 1991) p. 1045.
2 M. J. Zdeblick, R. Anderson, J. Jankowski, B. Kline-Schoder, L. Christel, R. Miles and M. Weber: Proc. Actuator 94 (Axon Technologie Consult GmbH, Bremen, 1994) p. 56.

3 T. Ohnstein T. Fukiura, J. Ridley and U. Bonne: Proc. IEEE MEMS 90 (IEEE, Piscataway, 1990) p. 95.
4 S. Messner, M. Muller, V. Burger and J. Schaible: Proc. IEEE MEMS 98 (IEEE, Piscataway, 1998) p. 40.
5 M. A. Huff, J. R. Gilbert and M.A. Schmidt: Proc. Transducers 93 (IEEE, Piscataway, 1993) p. 98.
6 M. Shikida and K. Sato: Journal of Microelectromechanical Systems **3** (1994) 76.
7 P. W. Barth, C. C. Beatty, L. A. Field, J. W. Baker and G. B. Gordon: Tech. Dig. Solid-State Sensor and Actuator Workshop (Cleveland, 1994) p. 248.
8 M. -J. Tsai, S. -C. Hsu, C. -H. Ke, R. -H. Jang and C. -Y. Wu: Proc. Actuator 98 (Messe Bremen GmbH, Bremen, 1998) p. 130.
9 J. Schaible, J. Vollmer, R. Zengerle, H. Sandmaier and T. Strobelt: Proc. Transducers '01 (Springer-Verlag, Berlin, 2001).
10 S. Messner: phD-thesis (Albert-Ludwigs-University, Freiburg, 2000).
11 J. Schaible: phD-thesis (University of Stuttgart,Stuttgart, 2001).
12 R. K. Gupta: phD-thesis (Massachusetts Institute of Technology, Cambridge, 1997).
13 W. van der Wijngaart, A. Thorsén and G. Stemme: Proc. IEEE MEMS 04 (IEEE, Piscataway, 2004) p. 233.
14 H. Sigloch: Technische Fluidmechanik (VDI Verlag, Düsseldorf, 1991) in Germany.
15 J. Wibbeler, G. Pfeiffer and M. Hietschold: Sens. Actuators A **71** (1998) 74.
16 H. Aine and B. Block: US patent US4585209, 1986.
17 M. Richter, S. Kluge: European patent EP0836012, 1998.
18 T. Wang, P. Barth, R. Alley, J. Baker, D. Yates, L. Field, G. Gordon, C. Beatty and L. Tully SPIE Proc. 3876 (SPIE, Bellingham, WA, 1999) p. 227.
19 A. K. Henning: Proc. Transducers 2003 (IEEE Press, Piscataway, 2003) p. 1550.
20 A. K. Henning: SPIE Proc. 5344 (SPIE, Bellingham, 2004) p. 155.
21 R. Zengerle, J. Wirtl and H. Frisch; Mikroventil: German patent DE19546181, 1997.

About the authors

Dr. Stephan Messner is the head of the microfluidics business unit at the HSG-IMIT (Institute for Micro- and Information Technology of the Hahn-Schickard-Gesellschaft) in Villingen-Schwenningen, Germany. His research is focused on microfluidics and covers topics like miniaturized and autonomous dosage systems, implantable drug delivery systems, lab-on-a-chip systems, microvalves as well as thermal sensors. Dr. Messner has a diploma in mechnical engineering from the Universtity of Stuttgart and a PhD degree in microsystems technology from the University of Freiburg, Germany.

Dr. Jochen Schaible is the head of the piezo technology devision of the Hoerbiger Automatisierungstechnik GmbH in Altenstadt, Germany. He is responsible for development, production and sales of piezoelectric actuated miniature valves for pneumatic applications. Before he joined Hoerbiger, Dr. Schaible worked for five years at HSG-IMIT on the development of electrostatic actuated microvalves. Dr. Schaible has a diploma in mechnical engineering and a PhD degree in microsystems technology from the Universtity of Stuttgart, Germany.

Prof. Dr. Roland Zengerle is the head of the Laboratory for MEMS Applications at the Department of Microsystems Engineering (IMTEK) at the University of Freiburg. In addition he is one of the directors at the HSG-IMIT (Institute for Micro- and Information Technology of the Hahn-Schickard-Gesellschaft) in Villingen-Schwenningen, Germany. His research is focused on microfluidics and covers topics like miniaturized and autonomous dosage systems, implantable drug delivery systems, nanoliter & picoliter dispensing, lab-on-a-chip systems, thermal sensors, miniaturized fuel cells as well as micro- and nanofluidics simulation. Dr. Zengerle co-authored more than 200 technical publications and 25 patents. He is the European editor of the Springer Journal of Microfluidics and Nanofluidics. Dr. Zengerle serves on the international steering committee of the IEEE-MEMS conference as well as on the technical program committee of the bi-annual Actuator conference.

Peter Nommensen received the diploma in physics from the University of Tübingen, Germany, in 1996. Thereafter he joined the HSG-IMIT in Villingen-Schwenningen, Germany, as a Process Engineer for PVD and bonding techniques. Since 2001, he is the head of the Department of Mikrotechnology at the HSG-IMIT. His current research interests include silicon micromaching and device integration techniques, with a focus on entire fabrication processes for MEMS applications and their suitability for serial production.